Laser-Induced Fluorescence Technique for the Quantification of Mixing in Impinging Jets

David R. Unger and Fernando J. Muzzio
Dept. of Chemical and Biochemical Engineering, Rutgers University, Piscataway, NJ 08855

A laser-induced fluorescence (LIF) technique is implemented to measure concentration profiles and mixing performance in two impinging jet geometries. Experimental results are reported for steady and unsteady (transitional) mixing of initially segregated miscible fluids. Flow structures are visualized by imaging concentration distributions at five vertical planes throughout the mixers. Mixing is quantified for each Reynolds number examined by calculating the overall intensity of segregation. Mixing performance varies substantially as a function of Reynolds number. Optimum operating conditions are identified for both impinging jet geometries. The results demonstrate the ability of laser-induced fluorescence to quantitatively capture small- and large-scale flow structures and accurately and reproducibly quantify mixing performance in real time for industrially-relevant mixing devices. The LIF technique proves to be an accurate and versatile method to quantify mixing performance of miscible fluids.

Introduction

Impinging jet mixers are widely used in industrial processes such as reaction injection molding (RIM), crystallizations and precipitations, and detergent neutralizations. Due to the rapid reactions that occur in these processes, inefficient mixing can lead to a chain of related undesirable consequences: desired reactions are slowed, selectivity is decreased, and the accumulation of unwanted byproducts is increased. Since the amount of byproducts is directly related to the scale of downstream purification and separation units (and the use of solvents in the purification units often entails additional costs due to environmental and regulatory concerns), it is clear that mixing has a large impact on both product quality and process profitability.

Over the years, many different techniques have been employed to examine the performance of impinging jets in an attempt to achieve a fundamental understanding of mixing in these systems. Malguernera and Suh (1977) evaluated mixing quality in an impinging jet mixer by measuring the standard deviation of a tracer in small aliquots taken from the mixer effluent. Though crude, this sampling method indicated that the jet Reynolds number (Re_j defined as $Re_j = (v_j D_j \rho/\mu)$, where v_j and D_j are the velocity and diameter of the entrance jet) was an important parameter for mixing performance. Tucker and Suh (1980) and Lee et al. (1980) used photography to analyze mixing in an impinging jet chamber, and found the transition from laminar to turbulent regimes above $Re_j = 50$. Lee et al. (1980) also used a fast exothermic reaction to identify a critical Reynolds number below which the polymerization rate is controlled by diffusion and above which kinetic control exists. Kolodziej et al. (1982) quantified mixing by using measurements of striation thickness distribution, adiabatic temperature rise, and molecular weight in a polyether polyol/butanediol/MDI, thermoplastic urethane system. They found that striation thickness measurements made using optical microscopy on the resultant polymer were more accurate than the other methods explored, and that average striation thickness decreased with increasing Re_j, for $Re_j = 80$, 250, and 450. Sandell et al. (1985) used a qualitative visualization technique to examine fluid mixing in different mixhead geometries and found that there was a decreasing rate of improvement over a Reynolds number range of 250−720. Akaike et al. (1986) also used dyed aqueous solutions to visualize the flow and observe fluctuations as a function of Reynolds number. Mahajan and Kirwan (1996) used the two-step Bourne reaction scheme in an impinging jet

Correspondence concerning this article should be addressed to F. J. Muzzio.

crystallizer to characterize micromixing for a range of jet diameters and jet Reynolds numbers. They also carried out the precipitation of Lovastatin and found that the level of micromixing in the precipitator affected crystal-size distribution when the time constant for micromixing was comparable to or larger than the induction time for nucleation of the solute.

Flow and mixing in impinging jets has also been studied using computational fluid dynamics (CFD) and computational fluid mixing (CFM) algorithms. Wood et al. (1991) and Johnson et al. (1996) have reported velocity field results using LDA and three-dimensional (3-D) numerical simulations that were qualitatively validated using LIF. They found that above $Re_j = 75$ the flow became unsteady and oscillations caused the jets to move off-center so that direct impingement no longer occurred. They also examined the effect of geometrical parameters (mixing changer diameter, head distance, and jet inlet position) on the flow field for $200 < Re_j < 500$. Unger et al. (1998) used PIV and CFD to examine the velocity fields and stretching characteristics for laminar flow impinging jets ($Re_j < 80$), and developed computational fluid mixing algorithms to simulate mixing for several impinging jet geometries. They found that while no mixing occurred for the steady flow of symmetric jets, mixing was improved substantially by slight modifications of the impinging jet geometry that disrupted geometric symmetry.

As computing power continues to increase and mixing simulations become more practical, it will be necessary to validate not only computational velocity fields (using LDA, LDV, PIV, and so on), but also mixing simulations. Moreover, experimental methods to evaluate mixing in real time would allow optimal mixing conditions to be determined for a mixer using dyed aqueous solutions, rather than expensive (and often hazardous) reactants.

The results presented in this study use a quantitative technique (planar-laser-induced fluorescence) to measure mixing performance in an impinging jet mixer for a wide range of Reynolds numbers and for two different impinging jet geometries. The technique allows non intrusive, real-time quantification of mixing to a spatial resolution limited only by the CCD camera pixel density ($O(10^5)$), and to a temporal resolution limited only by laser pulse rates ($\sim$ ms). Background and a brief review of the theory of laser-induced fluorescence are presented. The experimental setup and methods are described. Flow structures and mixing results for a standard impinging jet geometry (symmetric jets) and for a modified impinging jet geometry (asymmetric jets) are discussed. Finally, mixing is quantified as a function of Reynolds number by calculating the intensity of segregation, and used to predict overall reactor yield, thus allowing quantitative comparison between the two mixers.

Background and Theory

Applications of LIF were reviewed by Wild et al. (1987) and Walker (1987). LIF and its analogous 2-D counterpart, planar laser-induced fluorescence (PLIF), have been used by several researchers to instantaneously measure concentration fields. If 2-D measurements are taken in rapid succession, a pseudo-3-D concentration field may be approximated. The majority of LIF studies have been used to examine turbulent flows in liquids and gases (see, for example, Arcoumanis et al., 1990; Barrett and Van Atta, 1991; Buch and Dahm, 1996; Dahm and Dimotakis, 1987, 1990; Dahm et al., 1990, 1991; Distelhoff et al., 1997; Gaskey et al., 1990; Hassa et al., 1987; Koochesfahani and Dimotakis, 1985; Lozano et al., 1990; Muck et al., 1990; Nash et al., 1995; Westblom and Alden, 1989). LIF is effective for the study of small-scale flow phenomena under conditions such that laser absorption by the ambient fluid is minimal, so that a low power laser can produce high resolution visualizations. Therefore, it is well-suited for the study of turbulent mixing where it is necessary to accurately and rapidly measure fluctuating concentrations at a very small size scale.

The most attractive feature of laser-induced fluorescence is its ability to measure concentration fields in flow systems without the intrusion of a probe that would disturb the flow. LIF is based on the electronic excitation of molecules by an incident light beam and the measurement of the emitted light intensity. The components necessary for the experiment are a fluorescent species, an incident light source, and an optical system for measurement of the fluorescent emission. The fluorescent species is a molecule that absorbs a photon at a particular wavelength and, after a short time (smaller than a few ns), re-emits it at a longer wavelength. The fluorescence emission of the species can then be measured by recording the fluorescence with video recording, still photography, or CCD photography. The absorption and emission efficiency of three fluorescent dyes commonly used as tracers for concentration measurements in water flows was evaluated by Gaskey et al. (1990). They found that fluorescein is inferior to either Rhodamine B or Rhodamine 6G. For concentrations of Rhodamine B less than 0.08 mg/L, the response of fluorescent to the incident light is linear. Rhodamine B is used for this work, because its absorption spectrum (460−590 nm, max = 550) closely matches the available laser light wavelength (532 nm) and its emission spectrum (550−680 nm, max = 590) is almost completely separate from the laser light.

The absorption of light by fluorescent species is described by the Beer-Lambert law

$$\frac{dF}{dx} = -\epsilon CF \tag{1}$$

The fluorescence emission intensity I_e is then

$$I_e = -\Omega \frac{dF}{dx} \tag{2a}$$

or

$$I_e = \Omega\, \epsilon CF \tag{2b}$$

where Ω, the fraction of absorbed light emitted, is the quantum efficiency. It is necessary to filter out the wavelengths that correspond to the excitation beam so that scattered laser light does not interfere with the measurement. The effect of the filter on the emitted light can be taken into account using an optical efficiency term χ. Finally, the measured fluorescence signal is proportional to the volume of measure. Com-

bining these factors gives the measured intensity λ as

$$\lambda = \chi I_e V_m \tag{3a}$$

or

$$\lambda = \chi \Omega F \epsilon C V_m \tag{3b}$$

where χ is the optical efficiency term specific to the flow geometry of interest, Ω is the quantum efficiency, F is the incident radiation power, ϵ is the molar absorptivity of the dye, C is the actual dye concentration, and V_m is the measurement volume. The parameters Ω and ϵ are properties of the fluorescent compound, V_m and χ are determined by the optical arrangement, and F is determined by the laser power. When the laser sheet is of constant intensity across its cross-section, all these parameters are fixed, and

$$\lambda = AC(x,t) \tag{4}$$

It is obviously desirable to maximize the range of the measured signal intensity. Several parameters can be optimized in order to increase the measured signal intensity, but there are limitations on each of these parameters: (1) The maximum usable dye concentration is determined by the amount of light that is absorbed by the dyed fluid. If excess light is absorbed, the linear response of fluorescence intensity to concentration is lost. (2) The incident radiation power F is limited by the available laser power, and also must be moderated to minimize photochemical decomposition, which results in the destruction of the fluorescent compound and a decrease in the intensity of the emitted light. (3) The camera aperture size can be increased to its maximum diameter. (4) The exposure time of the camera can be increased up to a value of approximately one-fourth the pixel length divided by the maximum flow velocity. (5) An intensified CCD camera or low noise camera can be used, although improved camera quality increases camera cost (and overall system cost) substantially.

Methods

Two experimental geometries were examined, a symmetric jet mixer and a modified mixer (Figure 1). The mixers were constructed with glass, and are identical to those used in a previous study ((Unger et al., 1998), Case 0 and Case 5). The working fluid was a 60:40 glycerin:water mixture which had a density of 1.15 g/cm^3 and a viscosity of 0.01 Pa·s. The flow was gravity-fed to eliminate pulsation which commonly occurs with pumping. An overflow tank was used to provide a constant head source, and a flow rate was measured with a rotometer at the exit of the mixer. The mixers were enclosed in a rectangular glass box, which was filled with glycerin to reduce optical distortion.

The LIF setup is shown in Figure 2. A 10 mJ New Wave Research pulsed mini-YAG laser (Sunnyvale, CA) was used as the illumination source. The flow field was imaged using a DANTEC 80C42 Double Image 700 CCD camera (Mahwah, NJ). The mini-YAG laser produced a beam of 532 nm wavelength. Since the emission spectrum of Rhodamine B (the dye used in this study) was completely separate from the longest excitation wavelength of the laser, it was possible to use a single sharp-cut glass filter on the camera lens to remove reflections of the lower frequency laser light from the fluorescent signal to achieve a high signal-to-noise ratio. Three light filters (530 nm, 550 nm, and 570 nm) purchased from Schott Filter Glass (Duryea, PA) were tested for their efficiency to remove the laser light while detecting the fluorescent light emitted from the dye. It was found that the best filter for the present laser-dye combination was 550 nm.

Measurements were taken at five vertical cross-sections at 0.75 in. increments within the mixer (Figure 3). Vertical cross-sections were used rather than horizontal cross-sections, because in many mixing systems (such as stirred tanks) radial symmetry exists and segregation most often occurs in the axial direction. Thus, segregation in the mixer can be clearly observed within a single cross-sectional image. For each vertical cross-section, ten LIF measurements were taken at a rate of L/s. The FLOWMAP software package (DANTEC Measurement Technology, Mahwah, NJ) was used for data acquisition and laser/camera synchronization. Im-

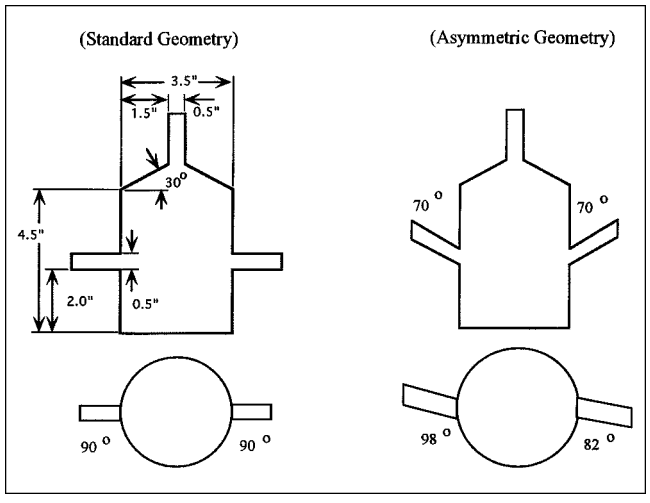

Figure 1. Standard (symmetric) and asymmetric impinging jet reactor geometries.

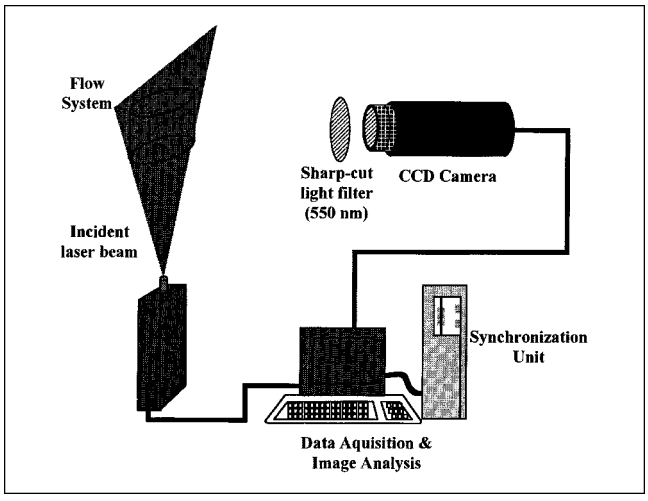

Figure 2. Laser-induced fluorescence apparatus.

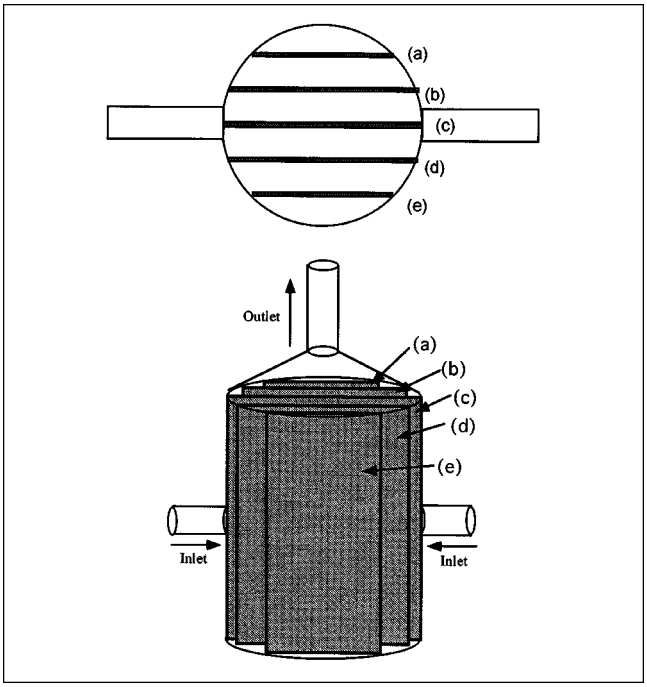

Figure 3. Locations of the five cross-sections examined in the impinging jets.

ages were captured using a CCD camera with 764×484 (369,776) light-sensitive pixels. The measuring volume per pixel depends on the camera magnification and the laser beam width. Since the largest cross-section (cross-section 4) had an area of 102 cm^2 and the beam width was approximately 1.0 mm, the measuring area per pixel was approximately 2.8×10^{-2} mm^2, and the measuring volume per pixel was approximately 2.8×10^{-2} mm^3. Images were saved as ASCII PBM files, which store light intensity values for each pixel on a grayscale from 0 (no light) to 255 (brightest light).

Results

Calibration

As it is desired to obtain a linear response of light intensity to concentration, it was necessary to determine the linear range for our specific laser, camera, and geometric setup. A simple test involves filling the mixer with different concentration dye solutions and measuring the emitted light intensity at each vertical plane in the mixer.

Figure 4 shows the emitted light intensity for ten dye concentrations. Light intensities reported in Figure 4 are the average pixel intensity for all five planes measured, and error bars represent the variance of the measured intensity. At zero dye concentration, no light is emitted from the illuminated plane, and the filter successfully filters out the incident light from the laser; thus, the measured emitted light intensity is zero. A linear range is obtained from 0.0 M to 1×10^{-6} M. Above a dye concentration of 1×10^{-6} M, a large portion of the incident laser light is absorbed by the fluid closest to the laser and the linear response is lost. Although the dynamic linear range could be improved by the modifications discussed earlier, the present laser-dye combination was capable of distinguishing approximately 100 concentration gradations, which is regarded as more than adequate to quantify mixing performance.

Standard impinging jet geometry

Mixing experiments were conducted by mixing a dyed jet (0.8×10^{-6} M Rhodamine B) with an undyed jet (0% Rhodamine B) at Reynolds numbers ranging $150 < Re_j < 600$. Representative examples of the LIF images obtained for the standard impinging jet geometry are shown in Figure 5 for a jet Reynolds number of $Re_j = 150$. Images shown in Figure 5 correspond to vertical cross-sections: (a) 1.5 in. behind the jet axis, (b) 0.75 in. behind the jet axis, (c) through the jet axis, (d) 0.75 in. in front of the jet axis, and (e) 1.5 in. in front of the jet axis. High dye concentration (high pixel light intensity) regions appear white, and zero dye concentrations appear black. The image taken at the center cross-section (Figure 5c) shows that direct impingement of the jets is still possible at $Re_j = 150$, although the jets are unstable and oscillations cause the jet streams to frequently move off-center. When direct impingement occurs, recirculation regions form below the jets (toward the closed end of the cylinder), similar to the patterns observed at low Reynolds numbers (Unger et al., 1998). Additionally, once the jets eventually move off-center, it is necessary to reduce the Reynolds number below $Re_j = 40$ to once again achieve direct impingement of the jets. Small and large eddies are present, and coarse mixing takes place in this flow, but there is still substantial large-scale segregation. In Figure 5, the dyed fluid jet (the left jet) is deflected upward (toward the mixer exit) and backward in the mixer, and the undyed fluid jet is deflected downward and forward in the mixer. As a result, the bottom and front regions of the mixer are characterized by a lower overall concentration of dye (a darker average color).

Image post-processing was carried out on the LIF images in Figure 5 in order to qualitatively determine mixing performance. First, the mean concentration of dye in the mixer was calculated by averaging pixel light intensity of all the images taken for a given Reynolds number. Then the concentration

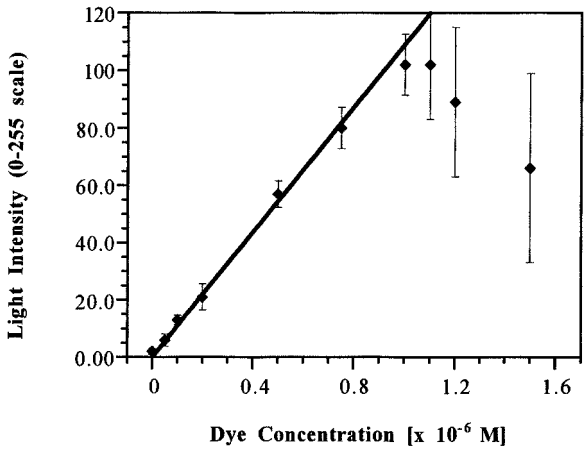

Figure 4. Calibration curve for pixel light intensity as a function of dye concentration.

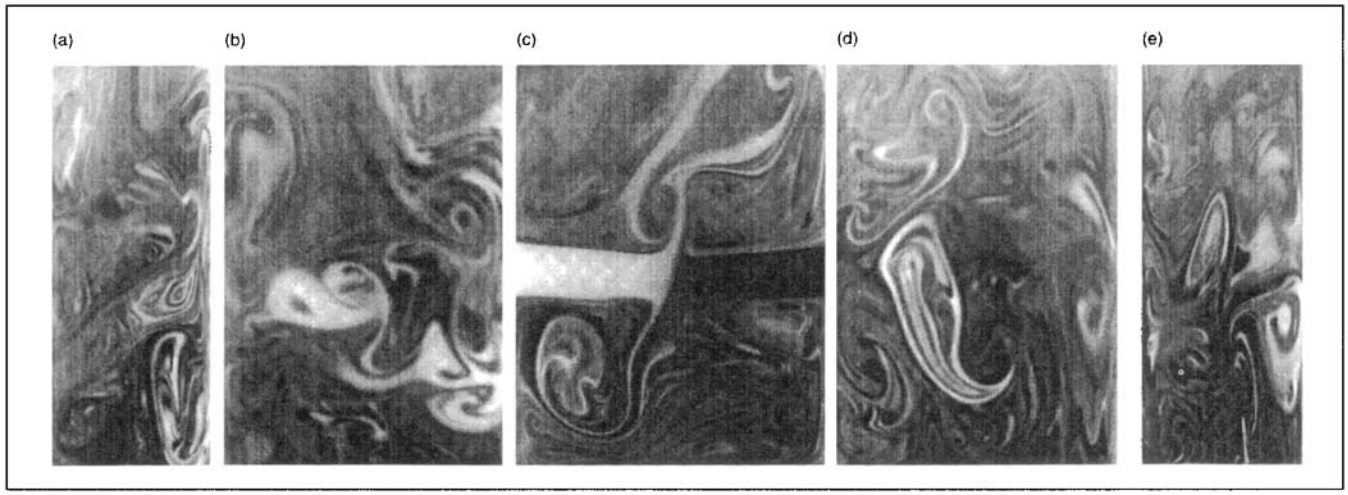

Figure 5. Symmetric jet geometry: sample LIF images for at $Re_j = 150$.

Cross-sections a–e correspond to vertical cross-sections depicted in Figure 3.

of each cross-section was normalized using the mean concentration, and images were reconstructed by assigning a RGB value to each pixel according to its normalized intensity. Regions of highest dye concentration were assigned red and yellow, and regions of lowest dye concentration were assigned blue, according to the color scale in Figure 6. On this scale, perfectly mixed regions appear as dark green. As shown in Figure 6, large regions of unmixed fluid (red and blue colors) exist in the mixer for $Re_j = 150$. Since the convective motion of fluid is slow in the bottom half of the mixer (below the jets), some of the fluid in the bottom of the mixer is entrained in recirculating regions, thus providing additional time for diffusion to complete the mixing process. Therefore, although some regions near the bottom of the mixer appear well-mixed (Figure 6b), the mixing *rate* in these regions may be much slower than required by the reactions of a given process. There is also some entrainment above the jets, which leads to improved mixing before the fluid exits the mixer.

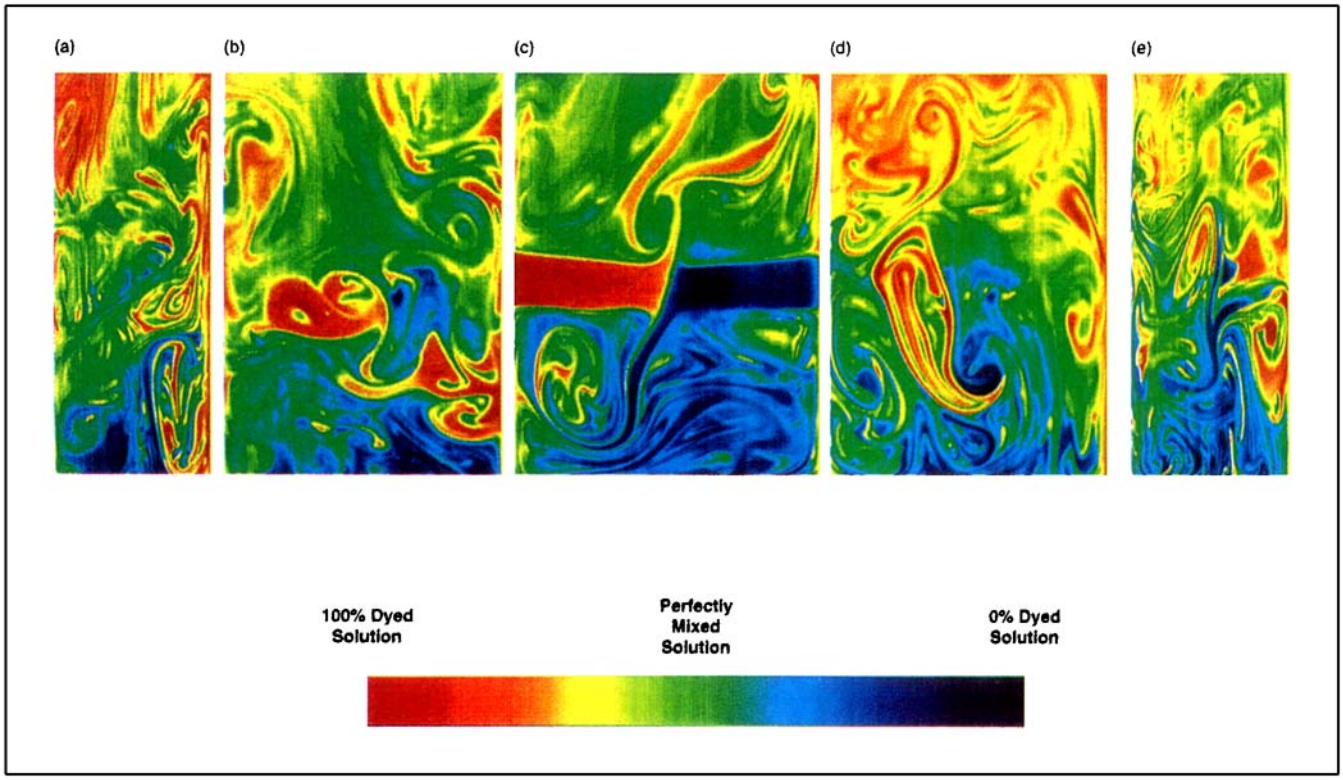

Figure 6. Symmetric jet geometry: post-processed "mixing intensity" images of the LIF images shown in Figure 5.

Colors range from red (100% dye solution) to dark blue (0% dye solution).

The post-processed LIF results of experiments performed at different Reynolds numbers are shown in Figure 7. In the interest of brevity, only the center cross-sections (c) are shown. Images represent Reynolds numbers of (a) 150, (b) 200, (c) 300, (d) 400, (e) 500, and (f) 600. As the Reynolds number is increased, direct impingement is no longer possible, and the frequency and amplitude of jet oscillations continuously increases. At $Re_j = 200$, flow structures are similar to those found at $Re_j = 150$. Large coherent structures are still present, and global segregation still exists between the two jet streams. Due to the higher frequency of oscillations at $Re_j = 200$, more small eddies are present, and homogeneity below and above the jets is increased. At $Re_j = 300$, the amplitude of the oscillations is so large that the jets frequently impinge on the opposite cylinder wall, where they split into several smaller streams. The oscillations also eliminate the recirculating regions above and below the jets. The only pure-component structures present above $Re_j = 300$ are the initial jet streams and the secondary flow caused by jet impingement on the cylinder wall. For Re_j above 400, the jets are no longer smooth and coherent, but exhibit turbulent structures as soon as they enter the mixer. As a result, rapid entrainment of the surrounding fluid occurs, and mixing efficiency is improved.

The improvement in mixing performance as Reynolds number is increased is also clearly shown in Figure 7. At $Re_j = 200$, mixing is improved slightly near the mixer exit (at the top of the mixer), and the red regions observed at $Re_j = 150$ are eliminated. Blue regions in the bottom of the mixer are also diminished, as the oscillations continuously sweep stagnant fluid out of this region. At $Re_j = 300$ through $Re_j = 600$, the number and size of unmixed regions are significantly decreased and the stagnation regions in the bottom of the mixer are almost completely eliminated. The size of well-mixed regions (dark green) increases continuously as Reynolds number is increased. At $Re_j = 600$, there are almost no pure component structures present except for the entrance jets and near the exit of the mixer.

Asymmetric jet geometry

LIF images are presented for the modified impinging jet geometry for a Reynolds number of $Re_j = 150$ in Figure 8. In this figure, images (a) through (e) represent the same cross-

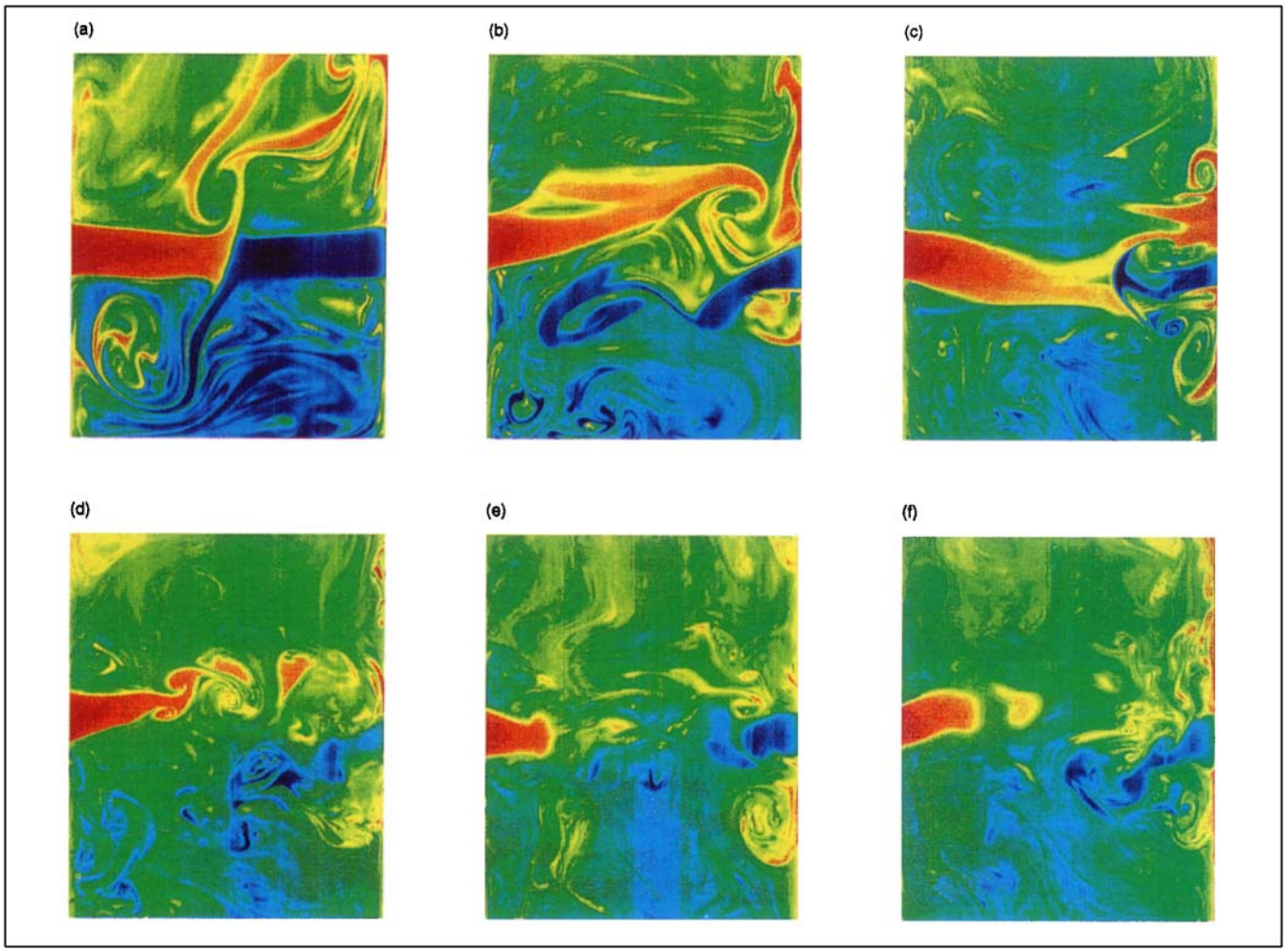

Figure 7. Symmetric jet geometry: post-processed LIF images as a function of Reynolds number.

Images correspond to the center cross-sections at jet Reynolds numbers of (a) 150, (b) 200, (c) 300, (d) 400, (e) 500, and (f) 600.

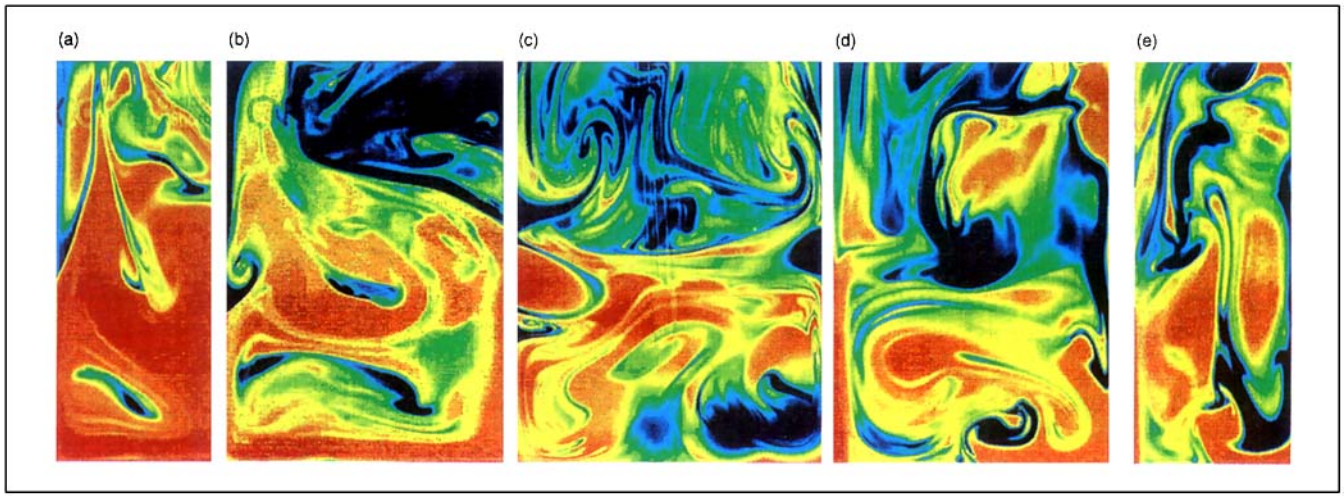

Figure 8. Asymmetric jet geometry: post-processed LIF images at $Re_j = 150$.

Cross-sections a–e correspond to vertical cross-sections depicted in Figure 3. Colors range from red (100% dye solution) to dark blue (0% dye solution).

sections as in Figure 5. High dye concentration (high pixel light intensity) regions appear red, and low dye concentrations appear blue. Direct impingement of the jets does not occur with this impinging jet geometry. As a result, the jet streams flow past each other and impinge on the opposite wall of the mixer. This flow causes a swirling motion to form in the bottom portion of the mixer, and increases convective motion below the jets. Consequently, the stagnant recirculation regions which were present for the standard geometry are no longer present. In their place, there are large eddies of both fluids at the bottom of the mixer. Since at $Re_j = 150$, the flow is still in the laminar regime and relatively steady in nature, there is also poor mixing in the top half of the mixer, near the mixer exit.

Mixing quality at $Re_j = 150$ is clearly illustrated for the modified geometry in Figure 8. In general, there is no heterogeneity for the modified geometry at $Re_j = 150$ than for the standard geometry at the same Reynolds number. The well-mixed regions (dark green) are much smaller, and the unmixed regions (reds and blues) are much larger. The jet oscillations that induced fluid mixing in the standard mixer have no effect on mixing for the modified geometry at $Re_j = 150$. Instead, mixing between the two streams occurs by the swirling motion that ensues at the bottom of the mixer. Although this swirling motion continuously stretches and folds the fluids (which is essential for good mixing) and increases their intermaterial area contact, the steady nature of the flow prevents material reorientation (which is also essential for good mixing).

LIF images for the modified geometry for a range of Reynolds numbers are shown in Figure 9. The images are again taken at the vertical cross-section through the jet axis (cross-section c), and represent the same Reynolds numbers as in Figures 7. As shown in these figures, the cross-over from laminar to "transitional" fluid motions occurs at a higher Reynolds number for the asymmetric jets than for the symmetric jets. This is because for symmetric jets, unsteadiness arises from the direct jet impingement (and consequent oscillations of the jets) at Reynolds numbers as low as 80. For the modified jet geometry, small-scale turbulent structures arise at the entrance of the jets to the bulk fluid only when the jet Reynolds number is increased to $Re_j = 400$. At this point, entrainment of the surrounding fluid causes more efficient global mixing. Additionally, by angling the jets downward, mixing in the bottom half of the mixer is improved substantially, as compared with the standard geometry. As shown in Figure 9e and 9f, there is good global homogeneity throughout the mixer, and the only unmixed fluid is observed either directly out of the jets or very near the exit of the mixer, where isolated mixing regions exist.

Quantification of mixing

While the previous diagrams provide a qualitative description of mixing efficiency, it is more beneficial to use these images to *quantify* mixture quality. Using the digitized images, the degree of mixedness was quantified using the "intensity of segregation" measure (Danckwerts, 1952). Intensity of segregation I is defined by

$$I = \frac{\sigma_a^2}{\bar{a}\cdot\bar{b}} \equiv \frac{\sigma_a^2}{\bar{a}(1-\bar{a})} \tag{5}$$

where the variance of species a is given by

$$\sigma_a^2 = \overline{(a-\bar{a})^2} \equiv \overline{a^2} - (\bar{a})^2 \tag{6}$$

$\bar{a}$ is the mean concentration and a is the concentration for each individual measurement. As mentioned earlier, 370,000 measurements (each with a volume of 2.8×10^{-2} mm^3) are generated from a single LIF image. As defined by Eq. 5, I has the value 1.0 when segregation is complete (that is, when the concentration of dye at every measurement point is 1 or 0), and the value 0.0 when the concentration is uniform. In general, I reflects the extent to which the concentration in

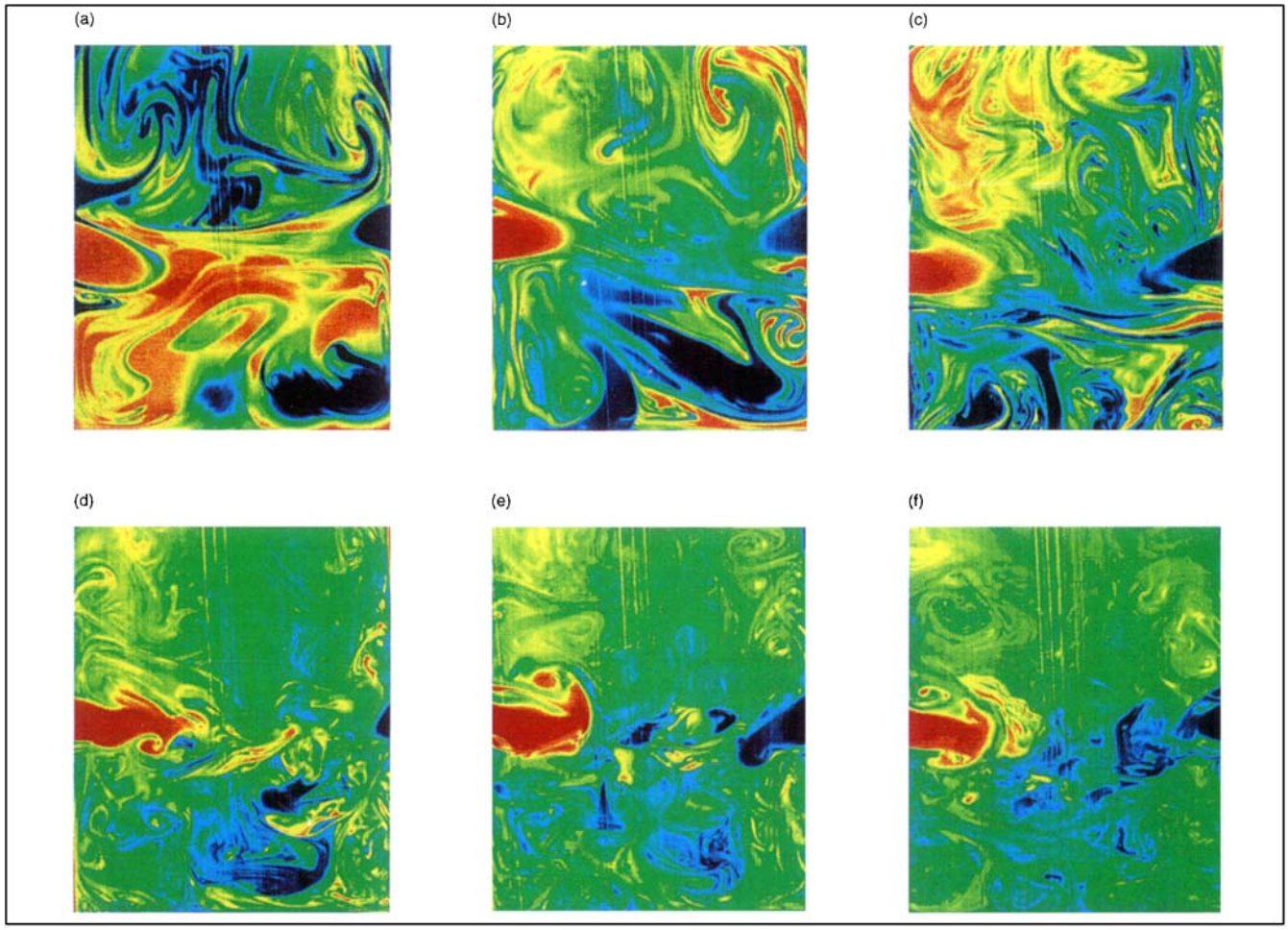

Figure 9. Asymmetric jet geometry: post-processed LIF images as a function of Reynolds number.

Images correspond to the center cross-sections at jet Reynolds numbers of (a) 150, (b) 200, (c) 300, (d) 400, (e) 500, and (f) 600.

different regions in the mixer departs from the mean. When two miscible liquids are mixed, the value of I is progressively reduced.

The intensity of segregation for each Reynolds number was averaged for each of the five cross-sections and ten repetitions. Therefore, the intensities of segregation shown in Figure 10 were calculated from approximately 10^7 concentration measurements. Examining the trend for the standard jet geometry, it is shown that the intensity of segregation drops off sharply from $Re_j = 150$ to $Re_j = 200$ decreases roughly linearly with jet Reynolds number from $200 < Re_j < 500$, and levels off for $Re_j > 500$. This trend is identical to those reported earlier by Tucker and Suh (1980) for a similar device. For the modified geometry, the intensity of segregation drops off sharply from $Re_j = 150$ to $Re_j = 300$, as the entrance jets become unsteady. Above $Re_j = 300$, the intensity of segregation is slightly lower in the modified impinging jet geometry due to greater homogeneity in the bottom of the mixer. Previous simulations (Unger et al., 1998) (data not shown) and experiments (Tucker and Suh, 1980; Unger et al., 1998) have shown that the intensity of segregation for standard jet geometries approaches 1.0 for $Re_j < 80$, whereas the intensity of segregation for the modified geometry remains relatively constant for $25 < Re_j < 150$ at approximately $I = 0.15$. This indicates that there are three regions where one mixer performs better than the other. For steady flows ($Re_j < 80$), the modified jet geometry provides much better mixing due to the swirling flow, as opposed to the symmetric jet geometry,

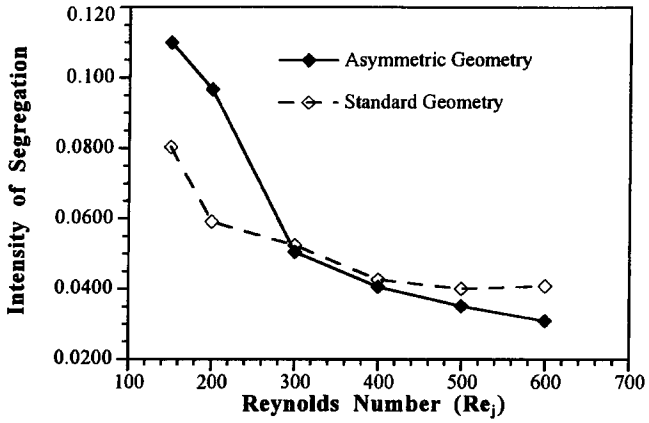

Figure 10. Intensity of segregation as a function of Reynolds number for the standard (– – –) and asymmetric (——) impinging jet geometries.

wherein no fluid mixing occurs. For unsteady-laminar flows ($80 < Re_j < 300$) the jet oscillations that prevent direct impingement of the fluids for the standard geometry (and thereby disrupt the spatial symmetry of the mixer) result in better mixing than the swirling motion of the modified jets. For unsteady-transitional flows ($Re_j > 300$), small isolated regions exist near the jet entrances as well as near the exit of the mixer. In general, both mixers perform well, although the modified geometry eliminates the dead region in the bottom of the mixer and results in slightly greater homogeneity.

Conclusions

The experiments shown here were used to *quantitatively* compare mixing performance between two impinging jet geometries: a standard (symmetric) geometry, and a modified geometry. Based on these results, three mixing regimes can clearly be identified for mixing in the impinging jet apparatus. For steady, laminar flows [$Re_j < 80$, results reported in Unger et al. (1998)], no mixing occurs in the standard geometry, and the modified jet geometry provides more efficient global mixing due to the swirling motion that ensues; these results are similar to those reported in a previous communication (Tucker and Suh, 1980). For unsteady-laminar flows ($80 < Re_j < 300$), the jet oscillations which occur in the standard geometry result in better mixing than the swirling motion of the asymmetric jets; flow for the asymmetric jets is mostly steady and similar to flow for $Re_j < 80$. For more highly unsteady flows ($Re_j > 300$), efficient mixing occurs in both geometries, although the asymmetric eliminates the dead region in the bottom of the mixer and results in slightly greater overall homogeneity.

A laser-induced fluorescence technique was successfully implemented to quantify concentration profiles and mixing performance in two impinging jet geometries. The technique is extended in this work to include quantification of mixing from the LIF images via the intensity of segregation. The technique is ideal for quantifying mixer performance in both laminar and turbulent regimes. The system requires only that the mixer be transparent from two directions at right angles to each other and that the working fluid is similarly transparent; the only system limitations are imposed by the pixel density of the CCD camera, and the repetition rate of the laser. In most cases, measurements can be taken at intervals as short as ms and spatial scales from less than 1 mm to more than 1 m. Post-processing of the LIF images allows: (1) identification of segregated/isolated regions in the mixer; and (2) calculation of standard mixing characterizations such as the scale and intensity of segregation. Current work is being carried out to extend the capability to include the calculation of more fundamental measures of mixing, such as the striation thickness distribution and intermaterial area density, and will be reported in future communications.

By identifying segregated regions in the flow, it is possible to make appropriate modifications in mixer geometry or process parameters in shorter times and avoiding wasting costly reactants. Additionally, intensity of segregation calculations allow direct quantitative comparison of different mixing devices or processing parameters. In summary, the laser-induced fluorescence technique demonstrated here has been shown to be an accurate, efficient, and versatile method for measuring mixing performance in model systems. Such measurements will be very valuable for developing fundamental knowledge about mixing processes, eventually facilitating *a priori* determination of process parameters and/or mixing criteria.

Literature Cited

Akaike, S., M. Nemoto, and R. Ishiwata, "Flow Visualization of Coaxial Impingement of Opposing Jets in a Mixing Chamber," Flow Visualization IV, Paris, France (1986).

Arcoumanis, C., J. J. McGuirk, and J. M. L. M. Palma, "On the Use of Fluorescent Dyes for Concentration Measurements in Water Flows," *Exp. in Fluids*, **10**, 177 (1990).

Barrett, T. K., and C. W. VanAtta, "Experiments on the Inhibition of Mixing in Stably Stratified Decaying Turbulence Using Laser Doppler Anemometry and Laser-Induced Fluorescence," *Phys. Fluids A*, **3**, 1321 (1991).

Buch, K. A. J., and W. J. A. Dahm, "Experimental Study of the Fine-Scale Structure of Conserved Scalar Mixing in Turbulent Shear Flows. Part 1. $Sc \gg 1$," *J. Fluid Mech.*, **317**, 21 (1996).

Dahm, W. J., and P. E. Dimotakis, "Mixing at Large Schmidt Number in the Self-Similar Far Field of Turbulent Jets," *J. Fluid Mech.*, **217**, 299 (1990).

Dahm, W. J. A., and P. E. Dimotakis, "Measurements of Entrainment and Mixing in Turbulent Jets," *AIAA J.*, **25**, 1216 (1987).

Dahm, W. J. A., K. B. Southerland, and K. A. Buch, "Four-Dimensional Laser Induced Fluorescence Measurements of Conserved Scalar Mixing in Turbulent Flows," *Applications of Laser Techniques to Fluid Mechanics*, R. J. Adrian, D. F. G. Durao, F. Durst, M. Maeda, and J. H. Whitelaw, eds., Lisbon, Portugal, Springer-Verlag, **1**, 3 (1990).

Dahm, W. J. A., K. B. Southerland, and K. A. Buch, "Direct, High Resolution, Four-Dimensional Measurements of the Fine Scale Structure of $Sc \gg 1$ Molecular Mixing in Turbulent Flows," *Phys. Fluids A*, **3**, 1115 (1991).

Danckwerts, P. V., "The Definition and Measurement of Some Characteristics of Mixtures," *Appl. Sci. Res.*, **3**, 279 (1952).

Distelhoff, M. F. W., A. J. Marquis, J. M. Nouri, and J. H. Whitelaw, "Scalar Mixing Measurements in Batch Operated Stirred Tanks," *Can. J. Chem. Eng.*, **75**, 641 (1997).

Gaskey, S., P. Vacus, R. David, J. Villermaux, and J. C. Andre, "A Method for the Study of Turbulent Mixing using Fluorescence Spectroscopy," *Exp. in Fluids*, **9**, 137 (1990).

Hassa, C., P. H. Paul, and R. K. Hanson, "Laser-Induced Fluorescence Modulation Techniques for Velocity Measurements in Gas Flows," *Exp. in Fluids*, **5**, 240 (1987).

Johnson, D. A., P. E. Wood, and A. N. Hrymak, "The Effect of Geometrical Parameters on the Flow Field of an Opposed Jet RIM Mix Head: Equal Flow and Matched Fluids," *Can. J. Chem. Eng.*, **74**, 40 (1996).

Kolodziej, P., C. W. Macosko, and W. E. Ranz, "The Influence of Impingement Mixing on Striation Thickness Distribution and Properties in Fast Polyurethane-Polymerization," *Poly. Eng. Sci.*, **22**, 388 (1982).

Koochesfahani, M. M., and P. E. Dimotakis, "Laser-Induced Fluorescence Measurements of Mixed Fluid Concentration in a Liquid Plane Shear Layer," *AIAA J.*, **23**, 1700 (1985).

Lee, L. J., J. M. Ottino, W. E. Ranz, and C. W. Macosko, "Impingement Mixing in Reaction Injection Molding," *Poly. Eng. Sci.*, **20**, 868 (1980).

Lozano, A., I. V. Cruyningen, P. Danehy, and R. K. Hanson, "Planar Laser-Induced Fluorescence Scalar Measurements in a Turbulent Jet," *Applications of Laser Techniques to Fluid Mechanics*, R. J. Adrian, D. F. G. Durao, F. Durst, M. Maeda, and J. H. Whitelaw, eds., Lisbon, Portugal, Springer-Verlag, **1**, 19 (1990).

Mahajan, A. J., and D. J. Kirwan, "Micromixing Effects in a Two-Impinging-Jets Precipitator," *AIChE J.*, **42**, 1801 (1996).

Malguernera, S. C., and N. P. Suh, "Liquid Injection Molding: 1. An Investigation of Impingement Mixing," *Poly. Eng. Sci.*, **17**, 111 (1977).

Muck, K. C., J. M. Wallace, and W. M. Pitts, "Simultaneous Real-

Time Line Measurements of Concentration and Velocity in Turbulent Flows,'' *Applications of Laser Techniques to Fluid Mechanics,* R. J. Adrian, D. F. G. Durao, F. Durst, M. Maeda, and J. H. Whitelaw, eds., Lisbon, Portugal, Springer-Verlag, **1**, 54 (1990).

Nash, J. D., G. H. Jirka, and D. Chen, ''Large-Scale Planar Laser Induced Fluorescence in Turbulent Density-Stratified Flows,'' *Exp. in Fluids,* **19**, 297 (1995).

Sandell, D. J., C. W. Macosko, and W. E. Ranz, ''Visualization Technique for Studying Impingement Mixing at Representative Reynolds Numbers,'' *Poly. Proc. Eng*., **3**, 57 (1985).

Tucker, C. L. I., and N. P. Suh, ''Mixing for Reaction Injection Molding. I. Impingement Mixing of Liquids,'' *Poly. Eng. Sci*., **20**, 875 (1980).

Unger, D. R., F. J. Muzzio, and R. S. Brodkey, ''Experimental and Numerical Characterization of Viscous Flow and Mixing in an Impinging Jet Contactor,'' *Can. J. Chem. Eng*., **76**, 546 (1998).

Walker, D. T., ''A Fluorescence Technique for Measurement of Concentration in Mixing Liquids,'' *J. Phys. E*, **20**, 217 (1987).

Westblom, U., and A. Alden, ''Spatially Resolved Flow Velocity Measurements Using Laser-Induced Fluorescence From a Pulsed Laser,'' *Opt. Let*., **14**, 9 (1989).

Wild, G., J. C. Andre, M. Grandclaudon, N. Midoux, and J. C. Charpentier, ''Methodes et Instrumentation Photophysiques pour le Genie des Procedes,'' *Entropie,* **137**, 69 (1987).

Wood, P., A. Hrymak, R. Yeo, D. Johnson, and A. Tyagi, ''Experimental and Computational Studies of the Fluid Mechanics in an Opposed Jet Mixing Head,'' *Phys. Fluids A*, **3**, 1362 (1991).

Manuscript received Sept. 29, 1998, and revision received June 1, 1999.